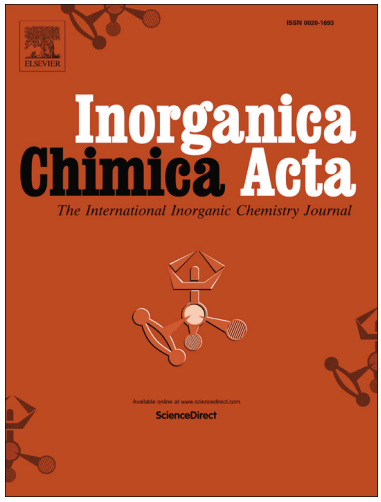

Research paper

Ni-thiosaccharinate complexes: synthesis, characterization and DFT studies. Biological properties as superoxide dismutase mimetics and as anti-carcinogenic agents

Fermín Delgado, Eva Nicova, Mariela Agotegaray, Verónica González Pardo, Viviana Dorn, Robert A. Burrow, Mariana Dennehy

PII: S0020-1693(19)30341-X
DOI: https://doi.org/10.1016/j.ica.2019.04.040
Reference: ICA 18885

To appear in: *Inorganica Chimica Acta*

Received Date: 14 March 2019
Accepted Date: 19 April 2019

Please cite this article as: F. Delgado, E. Nicova, M. Agotegaray, V. González Pardo, V. Dorn, R.A. Burrow, M. Dennehy, Ni-thiosaccharinate complexes: synthesis, characterization and DFT studies. Biological properties as superoxide dismutase mimetics and as anti-carcinogenic agents, *Inorganica Chimica Acta* (2019), doi: https://doi.org/10.1016/j.ica.2019.04.040

Ni-thiosaccharinate complexes: synthesis, characterization and DFT studies. Biological properties as superoxide dismutase mimetics and as anti-carcinogenic agents.

Fermín Delgado[a], Eva Nicova[a], Mariela Agotegaray[a], Verónica González Pardo[b], Viviana Dorn[a], Robert A. Burrow[c*], Mariana Dennehy[a*]

[a]INQUISUR/Departamento de Química, Universidad Nacional del Sur, Bahía Blanca, Argentina
[b]INBIOSUR/Departamento de Biología, Bioquímica y Farmacia, Universidad Nacional del Sur, Bahía Blanca, Argentina
[c]Departamento de Química, Universidade Federal de Santa Maria, 97105-900 Santa Maria, RS, Brazil

*Correspondence e-mail: mdennehy@uns.edu.ar; rburrow@ufsm.br

Abstract

This report describes the synthesis and characterization of two nickel thiosaccharinate complexes, $[Ni(tsac)_2(PPh_3)_2]$ (**1**) and $[Ni(tsac)_2(dppe)]\cdot CH_3CN$ (**2**), where tsac = thiosaccharinate anion, PPh_3 = triphenylphosphane and dppe = bis(diphenylphosphanyl)ethane. Elemental analysis, FTIR, ^1H, ^{13}C and ^{31}P NMR spectra and single crystal X ray diffraction studies of the complexes are presented. DFT optimizations of the two new compounds were performed in order to verify the FTIR vibrational assignations. The two nickel(II) thiosaccharinate complexes consist of mononuclear units in which the Ni atoms are the centre of square-planar coordination spheres, surrounded by two sulfur thiosaccharinate atoms and two phosphorous atoms from the phosphane ligands. In both complexes, the anions are mono-coordinated to the metal. In the $[Ni(tsac)_2(PPh_3)_2]$ structure, the phosphane moieties are located in *trans* position. In the $[Ni(tsac)_2(dppe)]$ structure, the dppe ligand chelates to the metal centre, as expected. Additionally, the superoxide dismutase (SOD) mimetic activity of the complexes was measured and it is reported herein. The effects of the complexes on cell proliferation were also studied and are described.

Keywords: Nickel, thiones, phosphane, crystalline structure, superoxide dismutase mimetic activity, cell proliferation inhibition

1. Introduction

Thionate ligands are considered poly-functional due to their ability to coordinate to metal centres either via a hard nitrogen atom or a soft sulfur atom and can adopt many coordination modes to form complexes of diverse nuclearity from monomeric to polymeric [1,2]. Thionate complexes have been used in a wide range of different applications going from the treatment of rheumatoid arthritis to anti-carcinogenic properties [3]. Coordination chemistry of heterocyclic thiones, usually in their deprotonated form, remains well studied, particularly for their potential biological use [4–9]. Some thione-metal complexes present mimetic metalloenzyme active site properties. Metalloenzymes – the proteins that contain a metal atom or metal clusters in their structures – are involved in a wide range of important biological processes. One class of metalloenzymes is the superoxide dismutases (SOD) which are present in all aerobic organisms. Their crucial function is devoted to combat oxidative stress. The anionic superoxide radical ($O_2^{\cdot-}$) is formed during aerobic respiration due to reduction of O_2 in the mitochondrial matrix

and is responsible in generating oxidative stress, which is implicated in several diseases such as diabetes, neurological disorders and post ischemic tissue injury [10]. Diverse types of SOD are known, including Cu/Zn-SOD [11], Mn-SOD [12] and Fe-SOD [13]. A new SOD enzyme has been discovered recently from *Streptomyces* soil bacteria which contains a Ni based active site [14]. The Ni environment appears as essential for catalytic activity because unlike other metals such as Cu or Zn, the Ni aqueous species does not react with $O_2^{\cdot-}$. The development of novel Ni-complexes with SOD activity is a current challenge considering their importance in potential use as SOD analogues in different pathologies. Reactive oxygen species (ROS) have shown to play an important role in viral oncogenesis. For instance, ROS-induction by Kaposi's sarcoma herpervirus promotes the proliferation and angiogenesis of endothelial cells [15]. Thus, targeting ROS production and their molecular sources could be an important therapeutic strategy.

Our recent laboratory research work has been devoted to the study of the thiosaccharine coordination. We have extensively explored the coordination of this thionate (the thioamide form of saccharinate) to different metals such as Cu, Ag, Au, Bi, Zn, Cd, Tl, Pd, Hg, and reported numerous metal-thiosaccharinate complexes so far [16 and references therein]. Currently, we have started working on the first transition row metal thiosaccharinates and have described interesting biological activity of Zn thiosaccharinates [17]. Ni^{II} complexes with monodentate phosphanes are used for different purposes, for example, for nickel-based catalysts. For that reason, several Ni-phosphane complexes are described in the literature [18–21].

There are, however, no nickel-thiosaccharinate complexes reported in the literature. For that reason, this work aims to expand the knowledge about thiosaccharinate chemistry, studying the coordination behaviour of nickel thiosaccharinates, and their response towards different biological activities, superoxide dismutase and cell proliferation inhibition. Two new thiosaccharinate Ni^{II} complexes with phosphane ligands, $[Ni(tsac)_2(PPh_3)_2]$ (**1**) and $[Ni(tsac)_2(dppe)]\cdot CH_3CN$ (**2**), where tsac = thiosaccharinate anion, PPh_3 = triphenylphosphane and dppe = bis(diphenylphosphanyl)ethane, were synthesized and well characterized, with their crystal structures determined. The superoxide dismutase mimetic activity for complexes **1** and **2**, determined through the XTT method, is presented. Both complexes presented the ability to inhibit XTT-formazan formation, revealing the capacity to induce superoxide radical dismutation. In addition, both complexes decreased Kaposi's sarcoma cell number, evidencing anti-proliferative properties.

2. Experimental

2.1. General remarks

All reagents were of commercial analytical quality and used without further purification. The protonated thiosaccharin (Hthiosaccharinate) was obtained as previously reported [22], using Lawesson's reagent (3.64 g; Fluka) and acid saccharin (3.00 g; Mallinckrodt) in toluene solution (25 mL) at 110 ºC. The FTIR spectra of the complexes were registered on a Thermo Scientific Nicolet iS50 FTIR-NIR spectrometer, employing KBr discs. Nuclear magnetic resonance (NMR) spectra were recorded on a Bruker ARX-300 spectrophotometer using the residual solvent peak or the deuterated solvent peaks as internal references for the ^1H NMR and ^{13}C NMR spectra, respectively. The ^{31}P NMR spectra were referenced to the signal of ^{31}P of an 85% H_3PO_4 solution as an external reference. The ^1H, ^{13}C and ^{31}P NMR studies were performed in DMSO-d_6 solutions. The C, H, and N elemental analyses were performed with a CE440 Elemental Analyzer.

2.2 Crystallography

Single crystal X-ray diffraction Data Collection of **1, 2** and **3** were performed on a Bruker D8 Venture single crystal diffractometer equipped with a Mo anode 50 W tube operating at 50 kV and 100 μA, Incoatec Montel X-ray focussing optics, Photon 100 CMOS detector and an Oxford Cryosystems Cryostream 800 temperature control system. Crystals were mounted on MiTeGen MicroMounts with polybutenes (M_n ~ 920). Data collection: Bruker APEX3/BIS [23]; cell refinement: Bruker SAINT [24]; data reduction: Bruker SAINT/SADABS [24,25]. Programs used to solve and refine structure: Bruker XT and XL (Bruker SHELXTL) [26,27]. Molecular graphics: Crystal Impact Diamond 3 [28] and Mercury CSD [29,30]. Table S1 summarizes crystal data, data collection procedures, structure determination methods and refinement results for complexes **1**, **2** and **3**.

2.3 Synthesis of the complexes

$[Ni(tsac)_2(PPh_3)_2]$ (**1**)

The $[Ni(tsac)_2(PPh_3)_2]$ complex was prepared by addition of a solution of $Ni(NO_3)_2{\cdot}6H_2O$ in acetonitrile (14.6 mg, 0.05 mmol, 2 mL) to an acetonitrile solution of PPh_3 (39.5 mg, 0.15 mmol, 2 mL) followed by a dropwise addition of a thiosaccharine solution (20 mg, 0.10 mmol, 2 mL in acetonitrile) (molar ratio:1:3:2). A red solid was then formed, filtered, washed with acetonitrile and collected. Yield: 52% (25.4 mg). Red crystals suitable for X-ray diffraction studies were produced by slow evaporation of a saturated solution of the compound in acetonitrile. When the reaction was held in a different molar ratio (metal:phosphane:thiosaccharine 1:2:2) the same complex was obtained. Calculated analytical percent composition for $C_{50}H_{38}N_2O_4P_2S_4Ni$: C = 61.295%; H = 3.909%; N = 2.859%; Found: C = 61.371%; H = 3.738%; N = 3.044%. Slightly soluble in dimethyl sulfoxide (DMSO) and dimethyl formamide (DMF). Very slightly soluble in acetonitrile. Non-soluble in other solvents (methanol, chloroform, dichloromethane, acetone, water).

$[Ni(tsac)_2(PPh_3)_2]$: ^{1}H NMR (300 MHz, DMSO) δ 7.82–7.96 (m, 1H, H3), 7.53–7.70 (m, 3H, H4/H5/H6), 7.37 (m, 9H, H10/H11/H12), 7.21 (m, 6H, H9/H13). ^{13}C NMR (75 MHz, DMSO) δ 191.82 (C1), 137.09 (C7), 136.95 (C8), 136.70 (C2), 133.50 (C13 or C9), 133.76 (C13 or C9), 132.41 (C4), 131.16 (C5), 129.37 (C11), 129.20 (C10), 129.12 (C12), 125.73 (C3), 119.52 (C6). ^{31}P NMR (121 MHz, DMSO) δ −6.90 (free PPh_3).

$[Ni(tsac)_2(dppe)]{\cdot}CH_3CN$ (**2**)

The complex was synthesized by addition of a dppe solution (40 mg, 0.10 mmol, 4 mL of CH_3CN) to a solution of $Ni(NO_3)_2{\cdot}6H_2O$ (14.6 mg, 0.05 mmol, 4 mL of CH_3CN) followed by a thiosaccharine solution (20 mg, 0.10 mmol, 4 mL of CH_3CN) (molar ratio: metal:thiosaccharine:diphosphane: 1:2:2), and kept under mechanical stirring at room temperature for one hour. The same compound was obtained when the molar ratio metal:thiosaccharine:diphosphane was changed to 1:2:1. The resulting yellow solid was filtered off and washed with cold acetonitrile. By slow evaporation of the mother solution orange single crystals appeared. They were washed with water and analysed using X-ray diffraction. Yield: 40.5%. Analytical percent composition calculated for $C_{42}H_{35}N_3O_4S_4P_2Ni$: C = 56.385%; H = 3.943%; N = 4.697%. Found: C = 55.848%; H = 3.713%; N = 4.157%. Very slightly soluble in

DMSO, acetonitrile and DMF. Non-soluble in other solvents (methanol, chloroform, dichloromethane, acetone, water).

$[Ni(tsac)_2(dppe)]\cdot CH_3CN$: ^{1}H NMR (300 MHz, DMSO) δ 7.08–8.18 (m, 14H, H3/H4/H5/H6/H9/H10/H11/H12/H13), 2.20–2.42 (m, 2H, H14). ^{13}C NMR (75 MHz, DMSO) δ 192.44 (C1), 137.67 (C8), 136.59 (C7), 135.54 (C2), 133.53 (C9/C13), 132.54 (C4), 132.42 (C5), 130.51 (C9/C13), 131.95 (C10), 131.72 (C12), 128.68 (C11), 124.87 (C3), 119.47 (C6), 26.41 (C14), 118.27 (CH_3CN), 1.19 (CH_3CN). ^{31}P NMR (121 MHz, DMSO) δ 61.36 (coordinated dppe); −14.56 (free dppe), 30.28 (oxidized dppe, $Ph_2(O)PCH_2CH_2P(O)Ph_2$).

$[Ni(tsac)_2(dppe)]\cdot 0.61(CH_3)_2CO$ (**3**)

During the crystallization attempts, 10 mg of the $[Ni(tsac)_2(dppe)]$ compound was dissolved in acetone. After slow evaporation of the solvent, orange crystals of $[Ni(tsac)_2(dppe)]\cdot 0.61(CH_3)_2CO$ were recovered. The crystals diffracted poorly. Compound **3** is isostructural to **2**, except for the change of the solvate molecule. The occupancy of the acetone solvate was refined to 61%. Details of the structure are in the Supporting Information.

2.4 Theoretical calculations

The theoretical calculations were performed with Gaussian09 [31]. The initial geometry optimization of complex **1** and **2** were performed with the semi empirical PM3 method. The geometry thus obtained was used as starting point for the density functional theory (DFT) calculations [32], that were performed with the B3LYP functional [33–35], which is known to be an appropriate methodology for the study on metal thiosaccharinate complexes with other co-ligands [16]. The zero-point energy was computed at the 6-31G** level for C, H, S, N and O atoms and employing the LANL2DZ effective core potential basis set for Ni. The characterization of the stationary point was done by Hessian matrix calculations of geometries obtained with full optimization for a minimum. The vibrational frequency analysis showed no imaginary frequencies for both complexes. All calculations were performed in gas phase. The structure figure (see Supplementary Info) was built with the VMD program.

2.5 Superoxide dismutase activity assay

The SOD-mimic activity for both coordination complexes was evaluated by an indirect method adapted from Štarha et al. [36]. The method is based on the reaction between XTT dye [2,3-bis(2-methoxy-4-nitro- 5-sulfofenyl)-2H-tetrazolium-5-carboxanilide natrium salt] (Aldrich) and superoxide anion ($O_2^{\cdot-}$). The interaction of XTT dye with superoxide anion radical leads to the formation of XTT-formazane, which presents maximum absorbance at 480 nm. The tested complexes, which would act as the scavengers for superoxide anion radicals, would decrease the absorbance. From this base, the required amounts of 1.00×10^{-3} mol L^{-1} solutions in N,N´-dimethylformamide (DMF) of the tested compounds were added to 1.0×10^{-2} M potassium phosphate buffer (pH 7.4) to provide 0.125, 0.250, 0.500, 0.750,1.00, 2.50, 5.00, 7.50 and 10.0 x 10^{-6} mol L^{-1} solutions. Subsequently, 500 µL of XTT dissolved in buffer were added. The resulting solution was mixed thoroughly. The reaction was started by the addition of 500 µL of a saturated KO_2 solution in DMF. Five replicates were tested for each concentration of both the complexes (n = 5). The absorbance at 480 nm was measured against a blank sample prepared without the XTT dye after 30 min of incubation at 37°C. The same procedure was used to pre-

pare the control sample without the complexes and the absorbance was measured against a solution containing only XTT dye. The percentages of inhibition (% INH) were determined according to the formula $(1 - X_{sample}/X_{control}) \times 100 \pm (S^2_{sample} + S^2_{control})^{½} \times 100\%$ where X is the media of the absorbance and S its standard deviation.

2.6 Cell line culture and proliferation assays

A cellular model of Kaposi's sarcoma was used. In this model, endothelial cell stably expresses the viral G Protein-coupled Receptor (vGPCR) transforming the cells to neoplastic. In this regard, vGPCR cells injected into immunosuppressed mice promotes tumour formation; thus, inducing angiogenic lesions similar to those developed in Kaposi's sarcoma [37,38]. These transfected cells were cultured in DMEM 5% foetal bovine serum (FBS) and selected with 500 µg/mL G418 (Cellgro, Manassas, VA). For proliferation studies, cells were seeded in 24-well plates at a density of 12,000 cells per well. After overnight growth, cells were treated with each ternary Ni^{II} complexes (**1** and **2**), vehicle (DMSO, 0.1%) or Htsac in duplicate during 24–48 h. At the end of the treatment, cells were harvested and counted in a Neubauer chamber; proliferation was quantified as the percentage of living cells [38].

3. Results and Discussion

3.1 Synthesis

The compounds $[Ni(tsac)_2(PPh_3)_2]$ (**1**) and $[Ni(tsac)_2(dppe)]\cdot CH_3CN$ (**2**) were easily synthesized by the addition of the phosphane ligand PPh_3 for **1** or dppe for **2** to a nickel(II) solution followed by two equivalents of the proligands, thiosaccharine, which readily deprotonated and complexed to the nickel centre. The initial reaction used an excess of phosphane ligand, 1:3 for **1** and 1:2 for **2**. However, after confirmation of the products, the stoichiometric reactions also produced the products.

3.2 Crystal structures

In Tables 1 and 2, some selected distances and angles of the complexes are highlighted. Complete crystallographic information for the complexes are provided in the crystallographic information files, available for download.

$[Ni(tsac)_2(PPh_3)_2]$ (**1**)

Compound **1** crystallized as a mononuclear square planar structure, Figure 1, with the nickel atom positioned over a crystallographic inversion centre. The asymmetric unit contains half of the complex: a half nickel atom to which are bound a thiosaccharide ligand via its exocyclic sulfur atom and a triphenylphosphane ligand. The inversion operation generates the other half of the complex, with the ligands necessarily in *trans* positions, and the thiosaccharinate ligands in an *anti* configuration to each other, by crystallographic symmetry to make a NiS_2P_2 core. The crystallographic symmetry also makes the core exactly planar. Usually Ni complexes containing ligands with sulfur atoms tend to form polynuclear S-bridge species [39], but also mononuclear complexes have been obtained depending on the selected co-ligands [40,41]. The thionate ligands are monoanionic when bound through their exocyclic sulfur atom to the nickel atom.

There is a minor distortion with one S1–Ni1–P1 angle (93.163(13)°) being slightly larger than the other, S1-Ni1-P1[a] = 86.837(13)°. The larger angle side features a π-π interaction between a phenyl ring of the phosphane ligand and the thiosaccharide system. Considering the six atoms (C11/C12/C13/C14/C15/C16) of the phenyl ring and nine atoms (N1/C1/C2/C3/C4/C5/C6/C7/S2) of the planar thiosaccharide system, the centroid-centroid distance is 3.83362(2) Å with the angle between the planes being 19.11(3) °. The side with the smaller angle, S1–Ni1–P1[a], has the thiosaccharide ligand fitting in the 'V' slot between two phenyl rings. The thiosaccharinate ligands bind at an angle to the Ni centre, with the Ni1-S1-C1angle = 110.03(5) °, close to the expected tetrahedral angle for a sp^3 hybridized S centre, and the plane of the ligand at an angle of 71.71(2) ° to the plane of the NiS_2P_2 core. The Ni–P bond distances (2.2474(4) Å) are slightly longer than the one reported for [Ni(L_1)(PPh_3)] (L1: 5-bromo-2-hydroxyacetophenone thiosemicarbazone, (2.209(1) Å) [42]. The phosphane ligands in *trans* positions usually have longer metal–P bond lengths; both are π acids receiving electrons from the same *d* orbital [43].

The S1–C1 bond length of the exocyclic S atom (1.7164(14) Å) is in the middle of the range of sulfur carbon double bond S=C (1.60 Å) vs S–C single bond (1.80 Å). It is lengthened due to the coordination to the metal which is noted when compared to the S–C bond distance in the free thiosaccharinate (1.622(6) Å) [44]. Moreover, the adjacent N1–C1 bond length of 1.3077(19) Å is found to be shorter than a C–N single bond (1.41 Å) but larger than a C=N double bond (1.29 Å). Compared to the C–N in the free thiosaccharinate (1.324(3) Å) it is slightly shortened. This value reflects de charge delocalization upon complexation. The gas phase DFT calculated values are similar to the experimental bond measurements, as can be seen in Table 1.

Table 1. Selected Bond and angles for complex [Ni($tsac)_2$($PPh_3)_2$] (**1**).

Bond lengths (Å)			Angles (°)		
Atoms	**Experimental**	**Theoretical**	**Atoms**	**Experimental**	**Theoretical**
Ni1–S1	2.2011(3)	2.2847	**S1–Ni1–P1**	93.163(13)	92.44
Ni1–P1	2.2474(4)	2.3669	**S1–Ni1–S1^a**	180	180
S1–C1	1.7164(14)	1.7237	**S1–Ni1–P1^a**	86.837(13)	87.56
S2–O1	1.4342(11)	1.4668	**P1–Ni1–P1^a**	180	180
S2–O2	1.4355(11)	1.4690	**Ni1–S1–C1**	110.03(5)	106.87
S2–N1	1.6682(12)	1.7052	**C24–C25–H25**	119.91†	121.16
S2–C7	1.7673(15)	1.7942	**C24–C25–C26**	120.17(14)	120.16
P1–C11	1.8233(14)	1.8490	**H25–C25–C26**	119.91†	118.90
P1–C21	1.8142(14)	1.8400	**C21–C26–C25**	120.16(14)	119.99
P1–C31	1.8200(14)	1.8424	**C21–C26–H26**	119.92†	120.17
N1–C1	1.3077(19)	1.3101			

[a]: symmetry operator = 1−*x*, 2−*y*, 1−*z*.

†: The hydrogen atoms are placed geometrically as the bisector of the C–C–C angles.

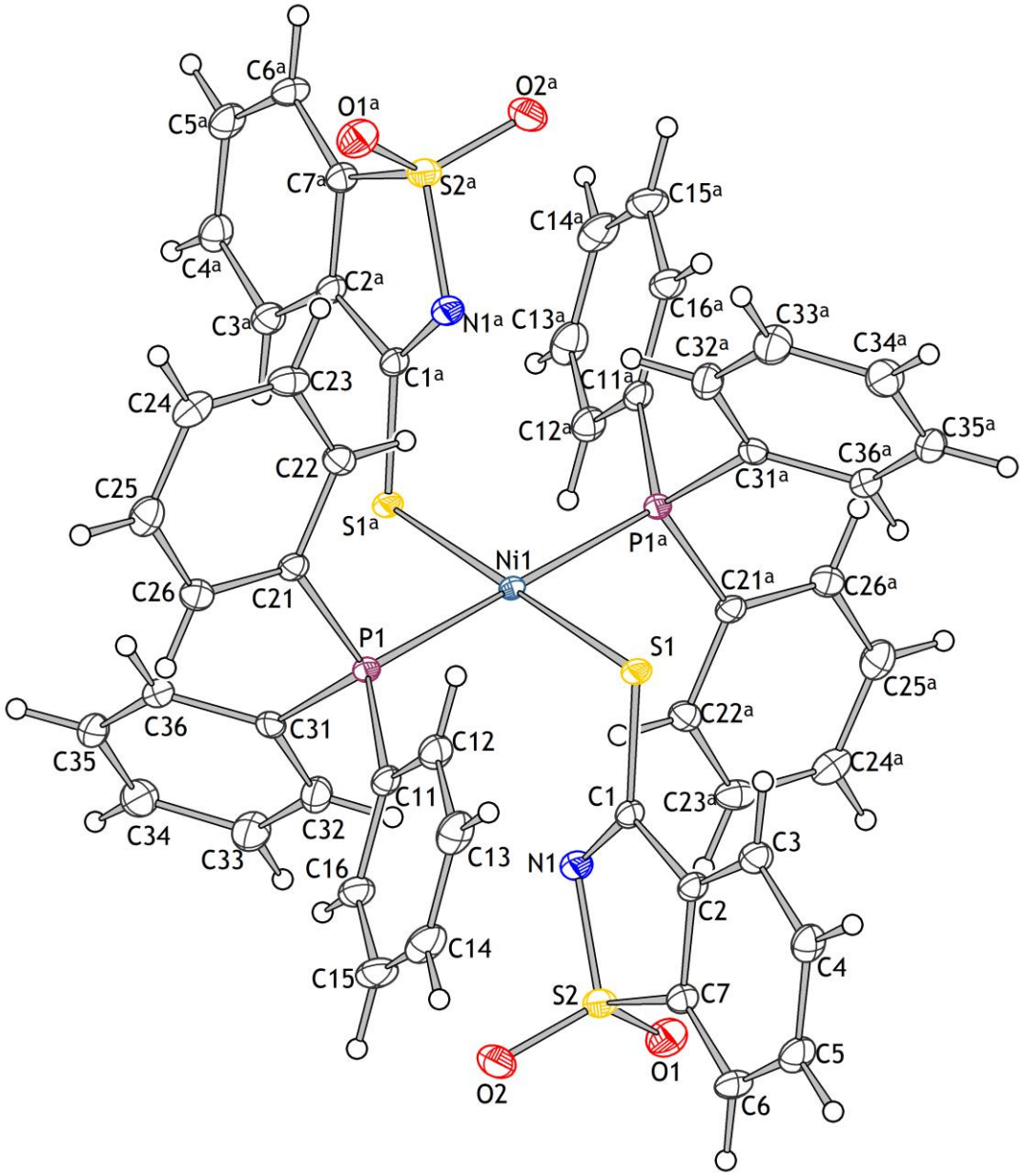

Figure 1. Molecular diagram of $[Ni(tsac)_2(PPh_3)_2]$ (**1**); symmetry operator [a]: 1−*x*, 2−*y*, 1−*z*.

$[Ni(tsac)_2(dppe)]\cdot CH_3CN$ (**2**)

Compound **2,** as **1,** crystallizes as a square planar mononuclear Ni^{II} complex, $[Ni(tsac)_2(dppe)]$, in the *cis* configuration, due to the κ^2-*P*,*P'* chelating dppe ligand, with a NiS_2P_2 core. The two thionate anions are bonded by their exocyclic sulfur atom, mono-coordinated, and in an *anti* configuration to each other. They are not chelating as for the thionate in the Ni complex reported by Hamaguchi *et al*., which contains a κ^2-*N*,*S* from the 2-pyS moiety [45]. The smallest angle results from the bidentate coordination of the diphosphane molecule (angles varying from 86.258(11) (P1–Ni1–P2) to 88.369(11), (S11–Ni1–P2), 89.573(11) (S21–Ni1–P1) and 95.803(11) (S11–Ni1–S21)). The geometric parameters τ_4 and τ_4' can be used to indicate the geometry around a four-coordinate metal centre with a value of 0 indicating square planar and

of 1, tetrahedral geometry [46,47]; the latter is more sensitive to geometric distortion. For **2**, the values of τ_4 and τ_4' are 0.068 and 0.064, respectively, signifying a very slight distortion from square planar geometry. Ni–P bond distances and Ni–S bond distances are in the expected range. Ni–P bond distances (2.1593(3) and 2.1653(3) Å) are shorter than those reported by Hamaguchi and some other related complexes (Ni–P bond length, 2.21 Å in average). In (**2**), the phosphane ligand, a π acid, is in the *trans* position to the sulfur atom, which is a weak π base, which should strengthen the Ni–P bonds, resulting in the shorter than average Ni–P bond lengths, as seen [43]. The longer Ni–S bonds, compared to those in **1**, are a result of an increase of the anionic character of the more electronegative exocyclic sulfur atom of the thiosaccharinate ligand [48], or an induced metal-ligand repulsion of the thiosaccharinate ligand by the rest of the molecule [49]. Selected bond distances and angles can be seen in Table 2.

Table 2. Selected Bond and angles for complex $[Ni(tsac)_2(dppe)]\cdot CH_3CN$ **(2)**

	Bond lengths (Å)			**Bond lengths (Å)**	
Atoms	**Experimental**	**Theoretical**	**Atoms**	**Experimental**	**Theoretical**
Ni1–S11	2.2453(3)	2.3158	**S22–O21**	1.4391(11)	1.469
Ni1–S21	2.2494(3)	2.3159	**S22–O22**	1.4364(10)	1.470
Ni1–P1	2.1593(3)	2.2621	**S22–N21**	1.6547(10)	1.698
Ni1–P2	2.1653(3)	2.2622	**S22–C27**	1.7639(11)	1.796
S11–C11	1.6976(11)	1.7169	**P1–C111**	1.8083(11)	1.831
S12–O11	1.4368(10)	1.469	**P1–C121**	1.8073(11)	1.833
S12–O12	1.4370(10)	1.470	**P1–C1**	1.8353(10)	1.867
S12–N11	1.6556(10)	1.698	**P2–C211**	1.8056(11)	1.831
S12–C17	1.7697(11)	1.796	**P2–C221**	1.8108(11)	1.833
S21–C21	1.6974(11)	1.716	**P2–C2**	1.8320(10)	1.867
N21–C21	1.3135(14)	1.314	**N11–C11**	1.3156(14)	1.314

	Bond angles (°)	
Atoms	**Experimental**	**Theoretical**
S11–Ni1–S21	95.803(11)	89.61
S11–Ni1–P1	174.611(11)	175.49
S11–Ni1–P2	88.369(11)	91.431
S21–Ni1–P1	89.573(11)	91.44
S21–Ni1–P2	175.808(11)	175.50
P1–Ni1–P2	86.258(11)	87.53
Ni1–S11–C11	95.08(4)	94.39
Ni1–P1–C111	111.77(4)	111.15
Ni1–P1–C121	116.44(4)	121.48
Ni1–P1–C1	109.87(3)	106.58

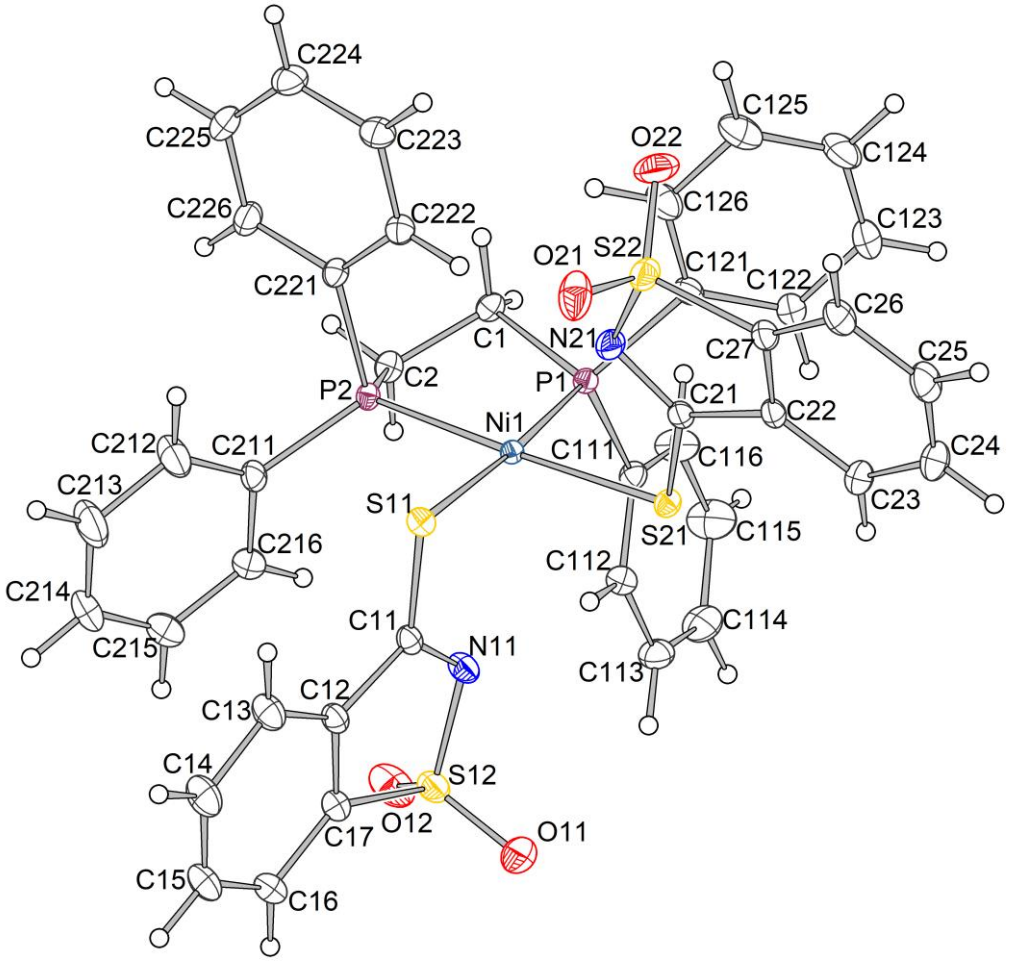

Figure 2. Molecular diagram of $[Ni(tsac)_2(dppe)]\cdot CH_3CN$ (**2**); the solvate molecule has been omitted for clarity.

3.3 Spectroscopic characterization.

The two complexes were characterized by spectroscopic and analytical methods. Adequate elemental analyses were obtained for both, thus confirming the nickel to ligand ratio and the purity of the complexes. With the aim to verify the vibrational band assignments in the gas phase, DFT/B3LYP method was chosen. The experimental spectra of the complexes can be seen in Figure 3. Table 3 shows some selected experimental and theoretical assignations of some characteristic vibrational bands. FTIR spectra of **1** and **2**, recorded on KBr discs, showed the expected vibrational bands of all the ligands (anions and phosphane moieties), shifted relative to the free species, and thus confirmed the coordination of the ligand to the metal centre. The spectra obtained for both complexes show the absence of a ν(NH) band at 3053 cm^{-1} due to loss of hydrogen from the protonated thione anions. Only signals of one thiosaccharinate were observed in the solid state FTIR of the two complexes, confirming that all anions are coordinated by the same way (that is mono-coordinated by the sulfur exocyclic atom). The bands due mainly to the ν(CS)δ(CNS) vibrational mode (appearing at 994 cm^{-1} in complex **1** and 1003 cm^{-1} in complex **2**) and to the ν(NS)δ(CCC) vibrational mode (appearing at 785 cm^{-1} in complex **1** and 801 cm^{-1} in complex **2**) reflects the rearrangement of the charge of the thiocarbonilic moiety upon complexation.

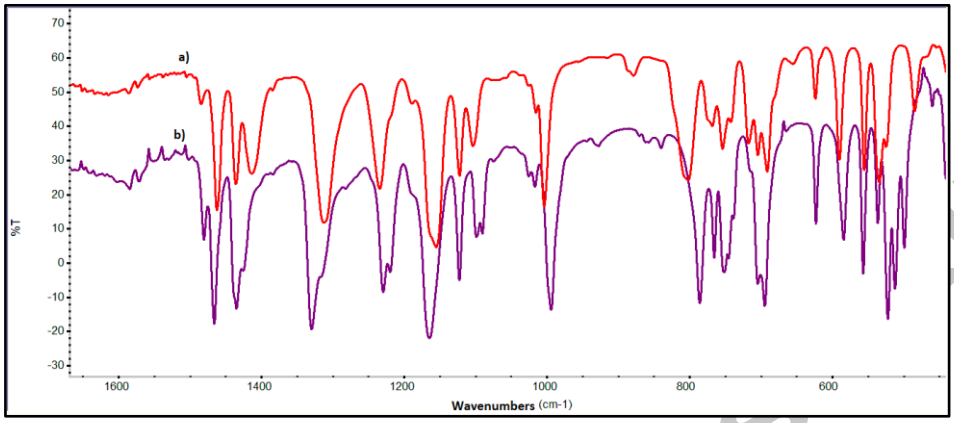

Figure 3. Experimental FTIR spectra of complex (a) **1** and (b) **2**.

Table 3. Selected vibrational bands for complexes **1** and **2**.

	1			**2**	
Vibration	Experimental	Theoretical	Vibration	Experimental	Theoretical
ν(CN) δ(ϕS)	1465s	1474	ν(CN) δ(ϕS)	1461s	1507
ν(CC)	1434m	1470	ν(CC)	1435m	1474
ν(CN) ν(ϕS)	1426w	Not seen	ν(CN) ν(ϕS)	1412m	1465
$\nu_{as}(SO_2)$	1329s	1307	$\nu_{as}(SO_2)$	1310s	1297
δ(CH) ν(CC)	1227m	1245	δ(CH) ν(CC)	1233m	1255;1253
$\nu_s(SO_2)$ ν(CC)	1164vs	1158	$\nu_s(SO_2)$ ν(CC)	1154s	1157
$\nu_s(SO_2)$ δ(ϕS)	1123w	1131	$\nu_s(SO_2)$ δ(ϕSN)	1120m	1127
ν(CS) δ(CNS)	994m	1007	ν(CS) δ(CNS)	1003m	1014
ν(NS) δ(CCC)	785m	768	ν(NS) δ(CCC)	801m	771
γ(CH)	766w	760	γ(CH)	766w	778
γ(CH) PPh_3	752w	754	γ(CH)dppe	752m	768
δ(CCC) PPh_3	692w	704	δ(CCC)dppe	690–718m	756
$\gamma(SO_2)$ δ(ϕCN)	623vw	631	$\gamma(SO_2)$	589m	546
$\gamma(SO_2)$	584vw	579	$\delta(SO_2)$ δ(CS)	555m	539
$\delta(SO_2)$ δ(CS)	555w	548	$\delta_\omega(SO_2)$	532m	519
$\delta_\omega(SO_2)$	521m	537	γ(CCC) dppe	485w	474
γ(CCC) PPh_3	439w	465	γ(CCC)	431w	1507
γ(CCC)	428w	434			

Codes: ν: stretching, δ: in plane bending, γ: out of plane bending, ϕ: benzenic ring, as: asymmetric, s: symmetric, vs: very strong, s: strong, m: medium, w: weak.
Normal modes wavenumbers calculated with B3LYP/6-31G** and LanL2DZ (Ni). No correction applied for the calculated values.

3.4 NMR

The room temperature NMR of both complexes **(1** and **2**) were recorded in DMSO-d_6 solutions, and the results were compared with the free ligands. The numbering scheme of the anions of complexes **1** and **2** are shown in Scheme 1.

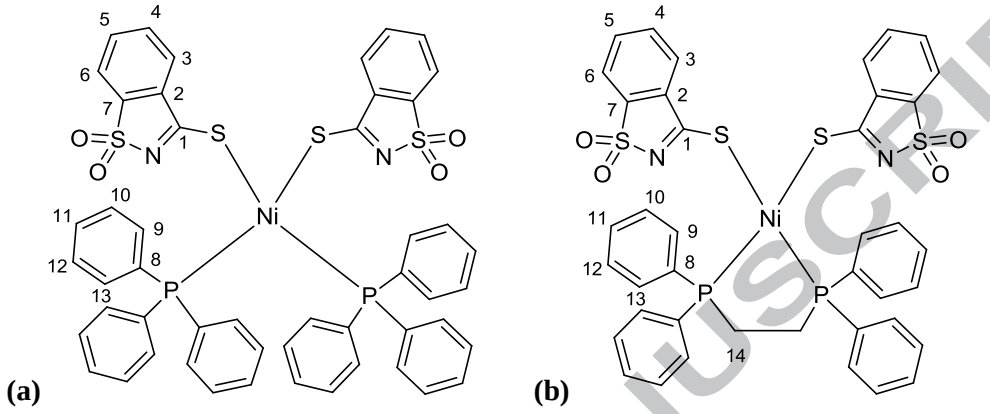

Scheme 1. NMR numbering of (a) $[Ni(tsac)_2(PPh_3)_2]$ (**1**) (b) $[Ni(tsac)_2(dppe)]\cdot CH_3CN$ (**2**)

The ^1H and $^{13}C\{^1H\}$ NMR data (in DMSO-d_6) for complexes **1** and **2** were consistent with the coordination of the thionate to the nickel centre. The complexes showed the characteristic signals of the aromatic protons of the ligands (PPh_3 and dppe) and the CH_2 signal (dppe) that appeared at δ 2.20–2.42 ppm. Regarding the thiosaccharinate protons, the SH(1) proton signal commonly appear at 6.42 ppm in the ^1H NMR spectrum of the free Htsac, although, in the ^1H NMR spectra registered of both complexes, there was no SH(1) signal; besides, nor has the NH(1) proton signal of the free Htsac appeared (commonly appear at around 9 ppm). Accordingly, these observations have been taken as indication that the Htsac molecule has coordinated to the metal centre as the thiosaccharinate ligand. The ^{13}C NMR spectra for complexes showed the expected chemical shifts of the coordinated thioamidic C1 atom around 190 ppm (C1 (**1**): 191.82 (**2**): 192.44). The signals are low-field shifted if compared with the chemical shift observed in the ^{13}C NMR spectrum for the free ligand (Htsac, C1 δ 161.5[50]). The ^{31}P NMR spectra showed that the complexes have been modified in the DMSO solution. The only signal in the ^{31}P NMR spectrum of (**1**) is that of the free PPh_3 molecule at −6.90 ppm. This peak and the lack of a peak for the complexed PPh_3 suggests that the ligand completely dissociates from (**1**) in DMSO. In the ^{31}P NMR of complex (**2**) there are three sharp resonances, corresponding to complexed dppe at 61 ppm, the free dppe at −15 ppm and the oxidized dppe at 30 ppm, probably caused by the DMSO. In order to obtain the complete assignation of the complexes' structures, we registered the 2D-HSQC NMR spectrum of complex **1** (which is slightly soluble in DMSO), but this has not been possible to complex **2**, because it is very poorly soluble in that solvent.

3.5 SOD mimetic activity

The superoxide dismutase mimetic activity for complexes **1** and **2**, determined through the XTT method, is presented in Figure 4. Both complexes presented the ability to inhibit XTT-formazan formation, revealing the capacity to induce superoxide radical dismutation. Assays were performed in DMF as previously done by our group [51]. The native Ni-SOD enzyme consists in a

hexameric assembly made of four helix bundles. Each subunit seems to operate independently of each other, and it is composed of a mononuclear Ni site.

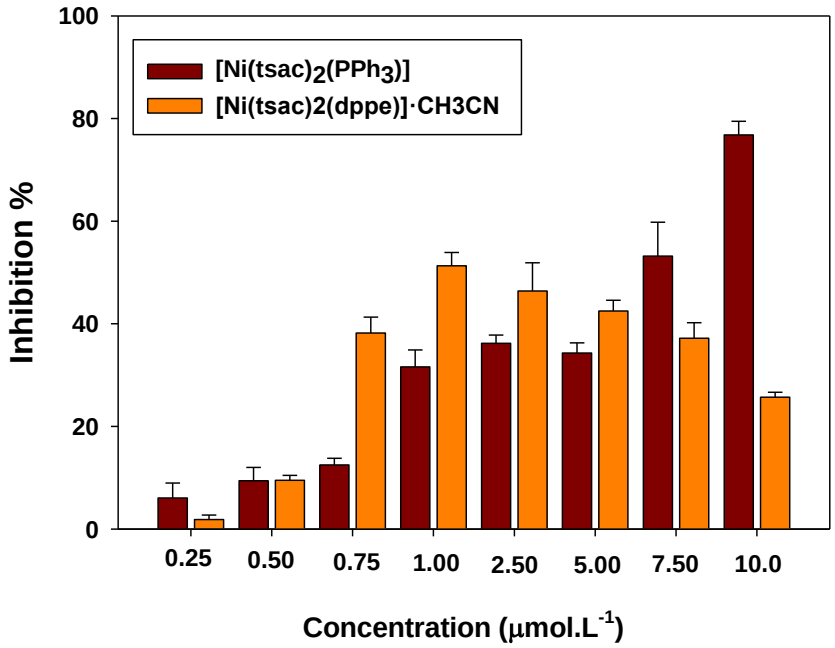

Figure 4. Inhibition of XTT-formazane formation by the coordination complexes under study, measured by XTT method.

In the case of the complexes in this study, the coordination sphere consists in a S_2P_2 environment. However, the complexes presented SOD-mimic activity. Ni environment appears as crucial for catalytic activity because unlike other metals such as Cu or Zn, the corresponding aqueous species does not react with $O_2^{\cdot-}$. The presence of S atoms would be responsible for the activity observed, since it is known that S environment imparts susceptibility to reactive oxygen species (ROS) [51] Considering that P atoms can act as donors, their presence would contribute to the activity of the active site of these complexes.

Even though **1** and **2** revealed SOD-mimetic activity, they behaved differently. Compound **1** showed increasing activity as a function of increasing the concentration. It achieved 77% of inhibition at the highest concentration tested (10 μM), presenting the best performance. Compound **2** initially showed lower activity compared to **1** and, as its concentration increased, its activity also increased, even in a greater proportion than **1**. In contrast to **1**, the activity of **2** decreased significantly for concentrations greater than 2.50 μM. These results can be justified analysing the correlation with the coordination sphere as catalytic centre of the complexes. Even both complexes present a catalytic centre based on S_2P_2 coordination sphere in the solid state, the spatial conformation is not the same, leading to a different behaviour against $O_2^{\cdot-}$ dismutation.

Considering the properties of the native enzyme, the reduced form of its active site contains a square planar Ni^{II} coordinating sphere to N_2S_2 environment, where thiolates are placed in *cis* conformation. During turnover, superoxide oxides Ni^{II}-N_2S_2 site, forming a five coordinate square-pyramidal Ni(III)-N_3S_2 via coordination with a neighbouring histidine residue (N_δ) in axial position, Scheme 2(a). Complex **1** active site is composed of S_2 environment, with S atoms in *trans* position. Ni–S distance (2.2011(3) Å) is similar to the observed in the native enzyme

(2.2–2.3 Å) meanwhile Ni–P (2.2474(4) Å) in solid state distance is longer than Ni–N bond length in the enzyme (1.9–2.1 Å), but in DMF solution the bond is lost [10]. Two N atoms are located on and under the Ni environment, giving the possibility to form the intermediate coordinated state Ni(III)-NS_2. In Scheme 2(b), the proposed oxidized and reduced forms are described for complex **1**. Scheme 2(c) shows the proposed structures for complex **2**. In this case, Ni environment presents a NiS_2P_2 structure with S in *cis* conformation, considering that there still are some coordinated dppe molecules in solution. This feature may be the responsible for the better performance than complex **1** in scavenging superoxide radical at intermediate concentrations. Due to distortion, Ni–S bonds are different in complex **2**: 2.2453(3) and 2.2494(3) Å but are similar in comparison to the enzyme. Ni–P distances (2.1593(3) and 2.1653(3) Å) are slightly longer than Ni–N in the native enzyme. In the same way as complex **1**, N atoms are available, but not strictly axially, to allow the five-coordination geometry state for the catalytic activity. Diverse factors govern the SOD-like activity of metal complexes such as exchange ability of the axial coordinated ligand, steric hindrance and flexibility on the active site to geometrical changes [52]. The differences observed in the catalytic activity for both complexes are ascribable to the fact that complex **1** is more flexible (considering that in solution PPh_3 are lost from the coordination sphere of the complex), facilitating $O_2^{\cdot-}$ binding. On the other hand, P–P bridging on complex **2** as exerted by dppe coordination would limit flexibility of the active site and steric hindrance might decrease the $O_2^{\cdot-}$ binding at high concentration thus reducing the catalytic activity.

(a) NiSOD active site from *Streptomyces coelicolor*

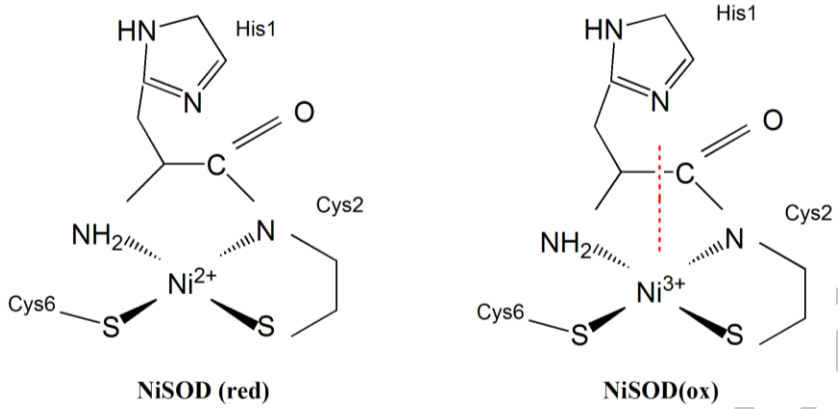

(b) [Ni(tsac)$_2$(PPh$_3$)$_2$]

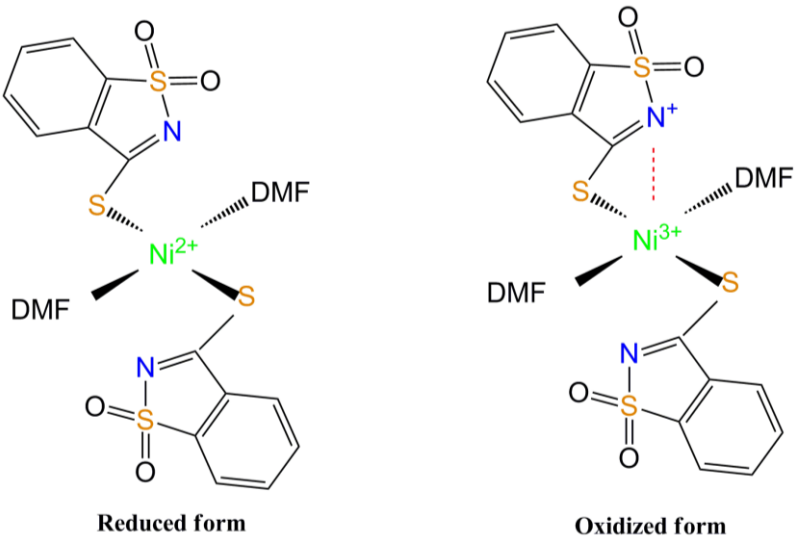

(c) [Ni(tsac)$_2$dppe]·CH$_3$CN

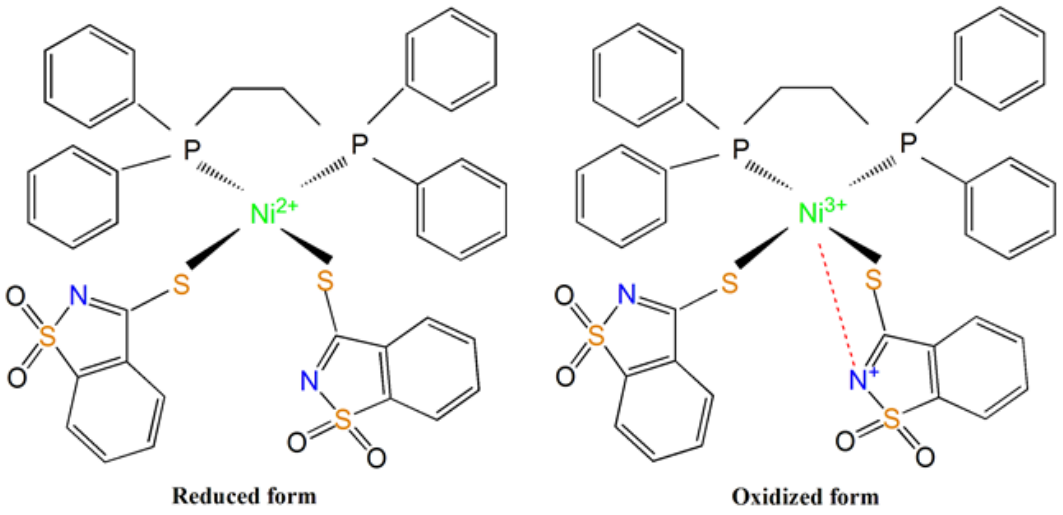

Scheme 2. (a) Structural changes in the active site for Ni-SOD during catalytic reaction [10]. (b) Possible mechanism proposed for **1** during turnover. (c) Structural properties of the active site proposed for **2**. In this case, steric hindrance due to dppe ligands is observable.

3.6 Cell line culture and proliferation assays

Cells were treated with each ternary Ni^{II} complexes (**1** and **2**) or Htsac in dose-response studies (1-3 µM) during 24 or 48 hours (Figure 5). Then, proliferation was measured as was described in Section 2.6 (Cell line culture and proliferation assays) and results were expressed as percentage of cell number of each complex or Htsac versus vehicle condition. As observed in Fig. 5 when Htsac was added, cell proliferation was not statically affected compared to control cells at 24 nor 48 hours, whereas both complex, **1** and **2**, triggered proliferation inhibition in a dose and time dependent manner. When complex **1** was employed, cell number decrease was significantly achieved when cells duplicated in time (20 hours approximately) at 48 hours, being 3 µM the more effective concentration. The complex in DMSO solution, as shown by the ^{31}P NMR, lost the PPh_3 ligands, so the effect can be attributed to the $[Ni(tsac)_2]$ complex. In addition, complex **2** has shown a similar behaviour than complex **1**, however, its antiproliferative actions were significantly achieved earlier at 24 hours.

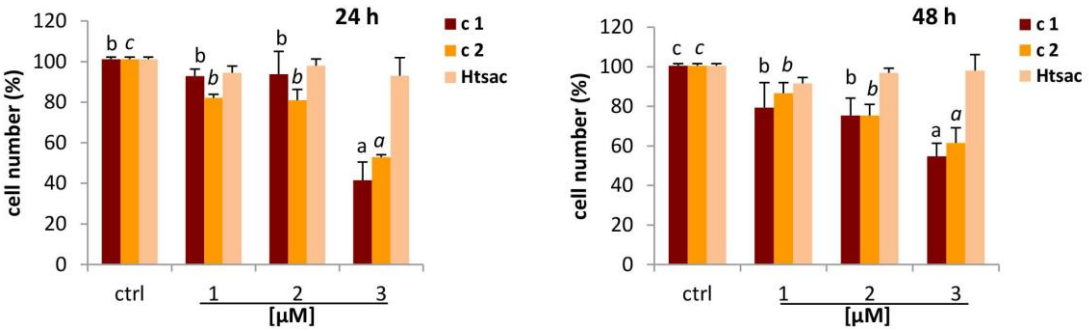

Figure 5. Cells were treated with 1–3 µM of each complex or Htsac or vehicle (DMSO) in DMEM 2% FBS for 24–48 h. Proliferation was calculated as percentage of leaving cells in treated conditions versus vehicle (ctrl). Percentage values (mean ± S.D.) were then represented in bar graphs. Statistical significance of data was first analysed by one way-ANOVA followed by Tukey test. Different letters for **1** and **2** (*italic*) indicate statistical differences (*p<0.05). Htsac ANOVA 24 h (p= 0.2773), Htsac ANOVA 48 h (p= 0.1819); n=6.

4. Conclusions

Two new Ni^{II} thiosaccharinates complexes were synthesized and characterized. Their crystal structures were determined by XRD and the results agree with the spectroscopic and elemental analysis of the complexes. Moreover, the DFT calculated structure in gas phase also agree with the experimental structures. Both compounds were monomeric, and the thionate was monocoordinated through exocyclic sulfur atom in the two of them.

Complex **1**, $[Ni(tsac)_2(PPh_3)_2]$, showed a moderate SOD activity. The difference between the SOD activity in complex **1** and **2** was attributed to the different coordination sphere in solution of both complexes. In addition, both complexes triggered cell proliferation inhibition in a dose and time dependent manner, whereas Htsac, with no complexation, had no effect. In this regard, further studies are needed to explore further the potential role of these complexes as anticancer drugs opening a new area of research.

5. Acknowledgements

M.D. and F.D. gratefully acknowledge the support of this project (Project M24/Q075) by SGCyT/UNS. M.A., V.D. and V.G.P. are researchers from CONICET (Consejo Nacional de Investigaciones Científicas y Técnicas, Argentina). F.D. is a fellow from CIC. R.A.B is grateful for a research fellowship from CNPq (Brazil) and support from CAPES (Brazil). The single crystal diffractometer was financed by a CT-INFRA grant (FINEP, Brazil).

6. Supplementary material

Crystallographic data for these structures has been deposited with the Cambridge Crystallographic Data Centre as supplementary data: CCDC numbers 1897300–1897302 for **1**–**3**. Copies of the data can be obtained free of charge upon request from The Director, Cambridge Crystallographic Data Centre, 12 Union Road, Cambridge CB2 1EZ, UK. (fax: +44 1233 336033; e-mail: deposit@ccdc.cam.ac.uk; WEB: http://www.csdc.cam.ac.uk). Additional information regarding ^{1}H and ^{13}C and HSQC NMR spectra for complexes, the coordinates, calculated frequencies and total energy in atomic units for the DFT calculations of the complexes are available as supplementary information.

7. References

[1] E.S. Raper, Complexes of heterocyclic thionates. Part 1. Complexes of monodentate and chelating ligands, Coord. Chem. Rev. 153 (1996) 199–255. doi:10.1016/0010-8545(95)01233-8.

[2] E.S. Raper, Complexes of heterocyclic thionates Part 2: complexes of bridging ligands, Coord. Chem. Rev. 165 (1997) 475–567. doi:10.1016/S0010-8545(97)90167-3.

[3] M.Y. Jomaa, M. Altaf, S. Ahmad, A. Alhoshani, N. Baig, A.-N. Kawde, G. Bhatia, J. Singh, A.A. Isab, Synthesis, characterization and anticancer evaluation of transplatin derivatives with heterocyclic thiones, Polyhedron. 141 (2018) 360–368. doi:10.1016/J.POLY.2017.12.016.

[4] M.S. Saini, A. Kumar, J. Dwivedi, R. Singh, A review: bilogical significances of heterocyclic compounds, Int. J. Pharma Sci. Res. 4 (2013) 66–77. http://www.ijpsr.info/docs/IJPSR13-04-03-005.pdf (accessed February 15, 2019).

[5] Ş.G. Küçükgüzel, P. Çıkla-Süzgün, Recent advances bioactive 1,2,4-triazole-3-thiones, Eur. J. Med. Chem. 97 (2015) 830–870. doi:10.1016/J.EJMECH.2014.11.033.

[6] A.A. A. Sulaiman, K.H. Omer, A.-N. Kawde, M.I. M. Wazeer, M. Altaf, M.M. Musa, S. Ahmad, A.A. Isab, Spectroscopic and Electrochemical Studies of the Interaction of Some Gold(III) Complexes with Biologically Relevant Thiones, Int. J. Chem. Kinet. 50 (2018) 178–187. doi:10.1002/kin.21149.

[7] S.M. Hiremath, A. Suvitha, N.R. Patil, C.S. Hiremath, S.S. Khemalapure, S.K. Pattanayak, V.S. Negalurmath, K. Obelannavar, S.J. Armaković, S. Armaković, Synthesis of 5-(5-methyl-benzofuran-3-ylmethyl)-3H- [1, 3, 4] oxadiazole-2-thione and investigation of its spectroscopic, reactivity, optoelectronic and drug likeness properties by combined computational and experimental approach, Spectrochim. Acta Part A Mol. Biomol. Spectrosc. 205 (2018) 95–110. doi:10.1016/J.SAA.2018.07.003.

[8] B. Mohammadi, F.K. Behbahani, Recent developments in the synthesis and applications of dihydropyrimidin-2(1H)-ones and thiones, Mol. Divers. 22 (2018) 405–446. doi:10.1007/s11030-017-9806-z.

[9] Z. Lu, Y.-Q. Yang, J.-H. Li, J.-N. Wei, Y.-Z. Wang, Convenient approach to chiral 4-monosubstituted 1,3-oxazolidine-2-thiones, Synth. Commun. 47 (2017) 2215–2219.

doi:10.1080/00397911.2017.1368083.

[10] E.P. Broering, P.T. Truong, E.M. Gale, T.C. Harrop, Synthetic Analogues of Nickel Superoxide Dismutase: A New Role for Nickel in Biology, Biochemistry. 52 (2013) 4–18. doi:10.1021/bi3014533.

[11] J.A. Tainer, E.D. Getzoff, J.S. Richardson, D.C. Richardson, Structure and mechanism of copper, zinc superoxide dismutase, Nature. 306 (1983) 284–287. doi:10.1038/306284a0.

[12] G.E.O. Borgstahl, H.E. Parge, M.J. Hickey, W.F. Beyer, R.A. Hallewell, J.A. Tainer, The structure of human mitochondrial manganese superoxide dismutase reveals a novel tetrameric interface of two 4-helix bundles, Cell. 71 (1992) 107–118. doi:10.1016/0092-8674(92)90270-M.

[13] D.L. Tierney, J.A. Fee, M.L. Ludwig, J.E. Penner-Hahn, X-ray Absorption Spectroscopy of the Iron Site in Escherichia coli Fe(III) Superoxide Dismutase, Biochemistry. 34 (1995) 1661–1668. doi:10.1021/bi00005a022.

[14] H.-D. Youn, H. Youn, J.-W. Lee, Y.-I. Yim, J.K. Lee, Y.C. Hah, S.-O. Kang, Unique Isozymes of Superoxide Dismutase inStreptomyces griseus, Arch. Biochem. Biophys. 334 (1996) 341–348. doi:10.1006/ABBI.1996.0463.

[15] Q. Ma, L.E. Cavallin, H.J. Leung, C. Chiozzini, P.J. Goldschmidt-Clermont, E.A. Mesri, A Role for Virally Induced Reactive Oxygen Species in Kaposi's Sarcoma Herpesvirus Tumorigenesis, Antioxid. Redox Signal. 18 (2013) 80–90. doi:10.1089/ars.2012.4584.

[16] R.A. Burrow, G.Z. Belmonte, V. Dorn, M. Dennehy, Three new Ag(I) thiosaccharinate complexes: Synthesis, structural studies, spectral characterization and theoretical analysis, Inorganica Chim. Acta. 450 (2016) 39–49. doi:10.1016/j.ica.2016.05.004.

[17] F. Delgado, E. Freire, R. Baggio, V. González Pardo, V. Dorn, M. Dennehy, Zn thiosacharinates: From ionic to polymeric structures. Synthesis, characterization and cell proliferation inhibition studies, Inorganica Chim. Acta. 479 (2018) 266–274. doi:10.1016/J.ICA.2018.04.040.

[18] X. Zheng, Q. Yang, Z. Li, Z. Zhu, X. Cui, H. Fu, H. Chen, R. Li, Trans-chloro-(1-naphthyl)bis[tris-(4-methoxyphenyl)phosphane]-nickel(II) catalyzed Suzuki-Miyaura coupling of aryl chlorides with phenylboronic acid, Catal. Commun. 57 (2014) 143–147. doi:10.1016/J.CATCOM.2014.08.010.

[19] K. Fang, L. Huo, L. Gao, L. Fan, T. Hu, Two Nickel(II) Coordination Polymers Based on Tri(*p* -carboxyphenyl) phosphane Oxide with Highly Selectively and Sensitively Detection of Acetone, Zeitschrift Für Anorg. Und Allg. Chemie. 644 (2018) 215–220. doi:10.1002/zaac.201700411.

[20] S.H. Schlindwein, M.R. Ringenberg, M. Nieger, D. Gudat, Synthesis and Spectroscopic Properties of "Charge-Inverted" Bis-benzenedithiolato Complexes of Copper and Nickel, Zeitschrift Für Anorg. Und Allg. Chemie. 643 (2017) 1628–1634. doi:10.1002/zaac.201700256.

[21] K.J. Cluff, N. Bhuvanesh, J. Blümel, Monometallic Ni ^{0} and Heterobimetallic Ni ^{0} /Au ^{I} Complexes of Tripodal Phosphine Ligands: Characterization in Solution and in the Solid State and Catalysis, Chem. - A Eur. J. 21 (2015) 10138–10148. doi:10.1002/chem.201500187.

[22] S. Scheibye, B.S. Pedersen, S. - O Lawesson, Studies on organophosphorus compounds XXI. the dimer of p- methoxyphenylthionophosphine sulfide as thiation reagent. a new route to thiocarboxamides, Bull. Des Sociétés Chim. Belges. 87 (1978) 229–238. doi:10.1002/bscb.19780870311.

[23] Bruker AXS Inc., APEX3 suite for crystallographic software - single crystal X-ray

diffraction, Madison, Wisconsin, USA., (2016).

[24] Bruker AXS Inc., SAINT+ Integration Engine, V8.38A, Madison, Wisconsin, USA., (2017).

[25] G.M. Sheldrick, SADABS, Version 2014/5, Bruker AXC Inc. (2014).

[26] Bruker AXS Inc., SHELXTL XT, Version 2014/5 - Crystal Structure Solution, Madison, Wisconsin, USA., (2014).

[27] Bruker AXS Inc., SHELXTL XL, Version 2017/1 - Crystal Structure Refinement, Madison, Wisconsin, USA., (2017).

[28] K. Brandenburg, H. Putz, Diamond, Version 3.2k - Crystal and Molecular Structure Visualization, (2016). http://www.crystalimpact.com/diamond.

[29] The Cambridge Crystallographic Data Centre (CCDC), Mercury CSD 3.10.3 (Build 205818), (2016).

[30] C.F. Macrae, I.J. Bruno, J.A. Chisholm, P.R. Edgington, P. McCabe, E. Pidcock, L. Rodriguez-Monge, R. Taylor, J. van de Streek, P.A. Wood, IUCr, *Mercury CSD 2.0* – new features for the visualization and investigation of crystal structures, J. Appl. Crystallogr. 41 (2008) 466–470. doi:10.1107/S0021889807067908.

[31] D.J. Frisch, M. J.; Trucks, G.W.; Schlegel, H. B.; Scuseria, G. E.; Robb, M. A.; Cheeseman, J. R.; Scalmani, G.; Barone, V.;Mennucci, B.; Petersson, G. A.; Nakatsuji, H.; Caricato, M.; Li, X.; Hratchian, H. P.; Izmaylov, A. F.; Bloino, J.; Zheng, G.; Sonnenber, Gaussian 09(C.01), Gaussian, Inc. Wallingford CT. (2009) 2–3. doi:10.2833/10759.

[32] W. Kohn, L.J. Sham, Self-Consistent Equations Including Exchange and Correlation Effects*, Phys. Rev. 140 (1965) A1133–A1138.

[33] C. Lee, W. Yang, R.G. Parr, Development of the Colle-Salvetti correlation-energy formula into a functional of the electron density, Phys. Rev. B. 38 (1988) 785–789.

[34] A.D. Becke, Density-functional exchange-energy approximation with correct asymptotic-behavior, Phys. Rev. A. 38 (1988) 3098–3100.

[35] B. Miehlich, A. Savin, H. Stoll, H. Preuss, Results obtained with the correlation-energy density functionals of Becke and Lee, Yang and Parr, Chem. Phys. Lett. 157 (1989) 200–206.

[36] P. Štarha, Z. Trávníček, R. Herchel, I. Popa, P. Suchý, J. Vančo, Dinuclear copper(II) complexes containing 6-(benzylamino)purines as bridging ligands: Synthesis, characterization, and in vitro and in vivo antioxidant activities, J. Inorg. Biochem. 103 (2009) 432–440. doi:10.1016/J.JINORGBIO.2008.12.009.

[37] S. Montaner, A. Sodhi, A. Molinolo, T.H. Bugge, E.T. Sawai, Y. He, Y. Li, P.E. Ray, J.S. Gutkind, Endothelial infection with KSHV genes in vivo reveals that vGPCR initiates Kaposi's sarcomagenesis and can promote the tumorigenic potential of viral latent genes, Cancer Cell. 3 (2003) 23–36. doi:10.1016/S1535-6108(02)00237-4.

[38] V. Gonzalez-Pardo, D. Martin, J.S. Gutkind, A. Verstuyf, R. Bouillon, A.R. de Boland, R.L. Boland, 1α,25-Dihydroxyvitamin D_3 and Its TX527 Analog Inhibit the Growth of Endothelial Cells Transformed by Kaposi Sarcoma-Associated Herpes Virus G Protein-Coupled Receptor *in Vitro* and *in Vivo*, Endocrinology. 151 (2010) 23–31. doi:10.1210/en.2009-0650.

[39] H.-B. Zhu, Y.-Z. Wei, L. Liang, Ni(II)/Cu(I) based coordination polymers with heterofunctional ligands integrating pyridine and pyrimidinethione structural motifs, Polyhedron. 109 (2016) 53–58. doi:10.1016/J.POLY.2016.01.051.

[40] S. Bharti, M. Choudhary, B. Mohan, S.P. Rawat, S.R. Sharma, K. Ahmad, Syntheses,

spectroscopic characterization, SOD-like properties and antibacterial activities of dimer copper (II) and nickel (II) complexes based on imine ligands containing 2-aminothiophenol moiety: X-ray crystal structure determination of disulfide Schiff bases, J. Mol. Struct. 1164 (2018) 137–154. doi:10.1016/J.MOLSTRUC.2018.03.041.

[41] B. Horn, C. Limberg, C. Herwig, B. Braun, Three-Coordinate Nickel(II) and Nickel(I) Thiolate Complexes Based on the β-Diketiminate Ligand System, Inorg. Chem. 53 (2014) 6867–6874. doi:10.1021/ic500698v.

[42] I. Kılıç-Cıkla, Ş. Güveli, T. Bal-Demirci, M. Aygün, B. Ülküseven, M. Yavuz, X-ray diffraction, spectroscopic and DFT studies on nickel(II)-triphenylphosphine complexes of 2-hydroxyacetophenone thiosemicarbazones, Polyhedron. 130 (2017) 1–12. doi:10.1016/J.POLY.2017.03.059.

[43] J.K. Burdett, T.A. Albright, Trans influence and mutual influence of ligands coordinated to a central atom, Inorg. Chem. 18 (1979) 2112–2120. doi:10.1021/ic50198a011.

[44] M. Dennehy, O.V. Quinzani, S.D. Mandolesi, J.A. Güida, G.A. Echeverría, O.E. Piro, Synthesis and spectroscopic characterization of two new thiosaccharinate salts. Molecular structure of bis(triphenylphosphine)iminium thiosaccharinate, PNP(tsac), Monatshefte Fur Chemie. 138 (2007). doi:10.1007/s00706-007-0648-8.

[45] T. Hamaguchi, R. Shimazaki, I. Ando, Synthesis and characterization of a heteroleptic nickel paddlewheel complex, J. Mol. Struct. 1173 (2018) 345–348. doi:10.1016/J.MOLSTRUC.2018.07.015.

[46] L. Yang, D.R. Powell, R.P. Houser, Structural variation in copper(I) complexes with pyridylmethylamide ligands: structural analysis with a new four-coordinate geometry index, s 4 †, (2007). doi:10.1039/b617136b.

[47] A. Okuniewski, D. Rosiak, J. Chojnacki, B. Becker, Coordination polymers and molecular structures among complexes of mercury(II) halides with selected 1-benzoylthioureas, Polyhedron. 90 (2015) 47–57. doi:10.1016/j.poly.2015.01.035.

[48] L.J. Manojlovic-Muir, K.W. Muir, The Trans-Influence of Ligands in Platinum(I1) Complexes. The Significance of the Bond Length Data, Elsevier Sequoia S.A, 1974. https://ac.els-cdn.com/S0020169300867079/1-s2.0-S0020169300867079-main.pdf?_tid=764381cc-14d5-42b4-a2ca-4f579d5de8b6&acdnat=1549476013_e23e5045d36975e04e235af256909fe8 (accessed February 6, 2019).

[49] B. Pinter, V. Van Speybroeck, M. Waroquier, P. Geerlings, F. De Proft, trans effect and trans influence: importance of metal mediated ligand–ligand repulsion, Phys. Chem. Chem. Phys. 15 (2013) 17354. doi:10.1039/c3cp52383g.

[50] M. Dennehy, G.P. Tellería, S.H. Tarulli, O. V. Quinzani, S.D. Mandolesi, J.A. Guida, G.A. Echeverría, O.E. Piro, E.E. Castellano, Synthesis and structural characterization of two new polynuclear metal thiosaccharinates: Hexakis(thiosaccharinato)hexasilver(I) and tetrakis(thiosaccharinato)tetracopper(I), Inorganica Chim. Acta. 360 (2007) 3169–3181. doi:10.1016/J.ICA.2007.03.016.

[51] M.A. Agotegaray, M. Dennehy, M.A. Boeris, M.A. Grela, R.A. Burrow, O.V. Quinzani, Therapeutic properties, SOD and catecholase mimetic activities of novel ternary copper(II) complexes of the anti-inflammatory drug Fenoprofen with imidazole and caffeine, Polyhedron. 34 (2012) 74–83. doi:10.1016/j.poly.2011.12.005.

[52] C.A. Grapperhaus, M.Y. Darensbourg, Oxygen Capture by Sulfur in Nickel Thiolates, Acc. Chem. Res. 31 (1998) 451–459. doi:10.1021/ar950048v.

[53] M.M. Ibrahim, A.E.-M.M. Ramadan, S.Y. Shaban, G.A.M. Mersal, M.M. Soliman, S. Al-Juaid, Thione-Based Nickel(II) Complexes as Functional Antioxidant Mimics: Scavenging Activity of Reactive Oxygen Species O2 −· and X-Ray Crystal Structure of

[Ni(Ttxyly)2]2 {Ttxylyl = Hydrotris(2-mercapto-1-xylyl-imidazolyl)borate}, J. Inorg. Organomet. Polym. Mater. 27 (2017) 1252–1263. doi:10.1007/s10904-017-0573-1.

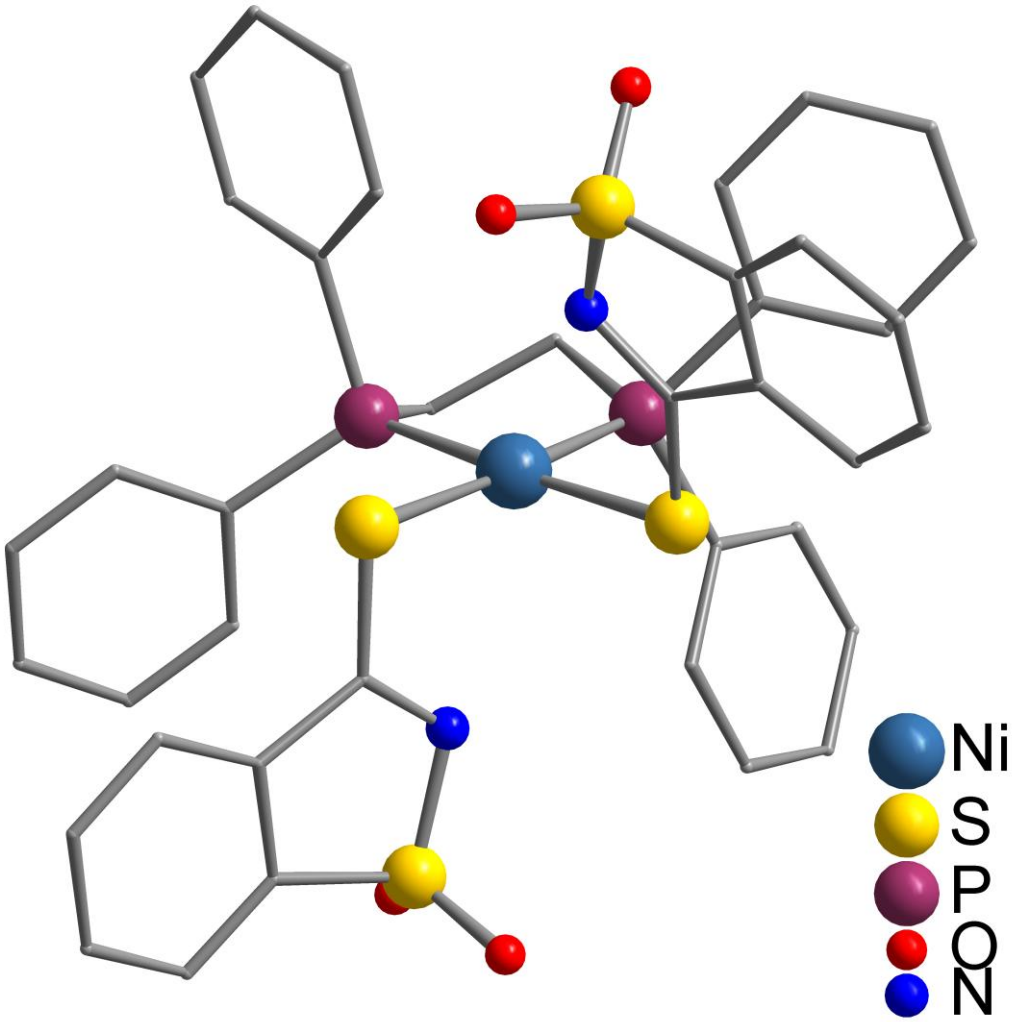

Ni-thiosaccharinate complexes: synthesis, characterization and DFT studies. Biological properties as superoxide dismutase mimetics and as anti-carcinogenic agents.

Fermín Delgado[a], Eva Nicova[a], Mariela Agotegaray[a], Verónica González Pardo[b], Viviana Dorn[a], Robert A. Burrow[c*], Mariana Dennehy[a*]

[a]INQUISUR/Departamento de Química, Universidad Nacional del Sur, Bahía Blanca, Argentina
[b]INBIOSUR/Departamento de Biología, Bioquímica y Farmacia, Universidad Nacional del Sur, Bahía Blanca, Argentina
[c]Departamento de Química, Universidade Federal de Santa Maria, 97105-900 Santa Maria, RS, Brazil

*Correspondence e-mail: mdennehy@uns.edu.ar; rburrow@ufsm.br

Highlights

- Two nickel thiosaccharinate complexes were synthesized.
- Their single crystal X-ray structures are reported.
- The complexes show moderate SOD mimic activity.
- The complexes triggered cell proliferation inhibition for Kaposi's sarcoma.